Energy Materials

Mini Review

The recent progress of single-atom catalysts on amorphous substrates for electrocatalysis

Cheng'ao Liu[1,2,#], Yanping Cui[1,2,#], Yao Zhou[1,2,*]

[1]Beijing Institute of Technology, Zhuhai Beijing Institute of Technology (BIT), Zhuhai 519088, Guangdong, China.
[2]Beijing Institute of Technology, Advanced Research Institute of Multidisciplinary Science, Beijing 100081, China.
[#]Authors contributed equally.

*Correspondence to: Prof. Yao Zhou, Advanced Research Institute of Multidisciplinary Science, Beijing Institute of Technology, Beijing 100081, China. E-mail: zhouyao@bit.edu.cn

Abstract

Single-atom catalysts (SACs) have emerged as a focal point in energy catalytic conversion due to their remarkable atomic efficiency and catalytic performance. The challenge lies in efficiently anchoring active sites on a specific substrate to prevent agglomeration, maximizing their effectiveness. Substrate characteristics play a pivotal role in shaping the catalytic performance of SACs, influencing the dispersion and stability of single atoms. In recent years, amorphous materials have gained attention as substrates due to their unique surface structure and abundance of unsaturated coordination sites, offering an ideal platform for capturing and anchoring single atoms effectively, thus enhancing catalytic activity. To clarify the interaction between single atoms and amorphous substrates, this review outlines amorphization methods, the mechanism of single-atom anchoring and the characterization methods of amorphous SACs. Subsequently, it summarizes the physical properties and electrocatalytic mechanisms of amorphous materials. Then, interactions between single atoms and amorphous substrates are categorized and summarized. Finally, the paper consolidates the research progress of amorphous SACs and outlines future development prospects. By exploring the synergistic relationship between single atoms and amorphous substrates, this review aims to deepen the understanding of their interaction mechanisms, thereby propelling advancements in SACs for energy catalytic conversion.

Keywords: Single atoms, amorphous substrates, interactions, electrocatalysis

INTRODUCTION

The increasing consumption of fossil fuels has highlighted environmental concerns, necessitating an immediate exploration of more sustainable and renewable energy sources[1]. Electrochemical conversion and storage devices, including water electrolyzers, rechargeable metal-air batteries and renewable fuel cells, currently form a vital component of the sustainability framework. They rely on a series of electrochemical redox reactions, such as hydrogen evolution (HER) at the cathode, oxygen evolution (OER) at the anode, oxygen reduction (ORR), and the electric reduction of carbon dioxide (CO_2RR)[2-4]. Consequently, there is an urgent need to develop efficient electrocatalysts to enhance electrochemical performance[5,6].

Special supported metal catalysts, known as single-atom catalysts (SACs), are characterized by the presence of all metal components in the form of single atoms dispersed on the substrate[7]. As the size of the metal center increases from single atoms to nanoclusters and nanoparticles, the energy levels become more continuous and approach the metallic state[8]. Unlike nanoclusters and nanoparticles, single atoms maximize the exposure of active sites, resulting in high atomic efficiency for catalysis. In larger nanoclusters and nanoparticles, there is greater orbital overlap between metal atoms, and the internal contribution of particles is stronger. In contrast, small clusters and single atoms, with fully accessible orbital structures, have a lower efficiency of orbital overlap between the metal center and the substrate[9]. Single atoms, however, offer advantages in this regard. Their electronic structure is directly influenced by the coordination environment, making it easily adjustable and more conducive to enhancing the efficiency of electrocatalytic reactions. A key scientific challenge concerning SACs revolves around understanding the stabilization mechanism of single atoms on the substrate[10]. Strong interactions or charge transfer between the metal single atoms and coordination substrates are essential to prevent atom aggregation into particles[11-14]. This necessitates the selection and optimization of suitable substrates to stabilize and disperse the target atoms effectively[15]. Therefore, the correct choice and optimization of substrates can significantly synergize with single atoms to enhance their catalytic efficiency and activity.

Amorphous materials possess higher specific surface areas, more active sites, and greater surface defects compared to crystalline materials. These characteristics contribute to their unique structures and distinctive surface chemical states in the field of electrocatalysis, playing a significant role in the adsorption of intermediates and catalytic activity. Typically, defects present in substrate materials play a crucial role in regulating the electronic structure and surface properties of single atoms[10,16]. Metal atoms can be effectively immobilized onto the surface by capturing them through substrate defects[17-19]. While crystalline material defects have been extensively studied, amorphous materials exhibit irregular internal particle arrangement and short-range order due to their lack of a crystalline structure. The relatively weak bonding energy of amorphous surface atoms results in abundant unsaturated coordination sites and dangling bonds[20,21]. This facilitates the absorption or binding of substances at the atomic scale. Additionally, amorphous materials boast a significant surface area, providing an increased number of active sites for anchoring single atoms. This abundance of additional reservoirs and potential active reaction centers serves to enhance catalytic behavior and electrochemical storage. Anchoring single atoms onto the surface of amorphous materials allows for precise control and localization of the active site, effectively avoiding the deactivation and aggregation of active sites and thereby enhancing the catalyst's activity[22,23]. Consequently, stabilizing metal single atoms using amorphous substrates emerges as an effective approach for developing highly efficient catalysts.

Based on the above analysis, amorphous materials possess unique characteristics for activating and stabilizing catalysts, while single atoms offer the advantage of maximizing atomic utilization. Therefore, investigating the preparation and mechanisms of catalysts anchored with single atoms on amorphous

materials is particularly crucial for future developments. This research can effectively support the subsequent development of high-performance and highly stable catalysts. In this review, as shown in Figure 1, we first provide an overview of general synthesis methods for amorphous materials and the mechanism of anchoring single atoms. Subsequently, the catalytic mechanism of amorphous materials is systematically explored. Finally, the anchoring mechanism of single atoms on amorphous substrates is discussed in detail, along with future prospects. This review presents a viable strategy for addressing sustainability challenges through the utilization of single-atom anchoring on amorphous materials.

PREPARATION OF AMORPHOUS MATERIALS, SINGLE ATOM ANCHORING METHODS AND CHARACTERIZATION TECHNIQUES

Synthesis methods of amorphous substrates

Due to the disordered atomic arrangement inherent in amorphous systems, these materials typically exhibit higher entropy compared to their crystalline counterparts, thus showing a propensity for crystalline transformation under external conditions[24]. Consequently, preventing or delaying the transition from amorphous to crystalline states remains a significant challenge, crucial for achieving controlled synthesis and precisely modulating the local structure of amorphous materials to enhance their efficacy in specific applications. Although the synthesis mechanisms of amorphous nanomaterials are not fully clear, there are still some similarities in the methods of preparing nanomaterials. Generally, several primary techniques are employed in the synthesis of amorphous materials.

Wet chemical method

Wet chemistry synthesis utilizes simple setups and readily available materials, ensuring operational ease, lower energy consumption, and scalability. By adjusting reaction conditions and ligand ratios, precise control over catalyst structure, morphology, and surface properties is achieved, meeting diverse catalytic needs. However, optimal catalytic performance often requires iterative optimization, potentially increasing time and cost. Wet chemical synthesis methods generally encompass solvothermal, ion exchange, and template-assisted approaches.

Leaching of ions occurs during wet chemical processes, resulting in structural changes. The gradual leaching of ions leads to local defects or distortions in the lattice structure. These defects and distortions form amorphous regions on the catalyst surface, gradually expanding and leading to the disordering of the overall crystal structure. For instance, Chen *et al.* subjected bulk-phase $LaNiO_3$ perovskite oxide to $FeCl_3$ solution, resulting in corrosion-induced amorphization[25]. Continuous leaching of large-sized La^{3+} ions led to the gradual collapse of the crystalline perovskite structure[25]. Similarly, Zhu *et al.* treated $NiMoO_4 \cdot H_2O$ pre-catalyst with an alkaline solution, resulting in the exfoliating from the bulk $NiMoO_4 \cdot H_2O$ nanorods due to the dissolution of Mo species and crystalline water. Alkaline etching and multi-step dissolution formed the superthin and amorphous $Ni(OH)_2$[26].

Heteroatom doping through wet chemical methods induces lattice distortion, resulting in partial or complete amorphization[27]. For instance, Kang *et al.* utilized dimethylamine borane and $NaBH_4$ as dual reducing agents and boron sources to generate three-dimensional mesoporous Ni-B amorphous alloy spheres [Figure 2A][28]. The selected-area electron diffraction (SAED) pattern [Figure 2B] confirms that the mesoporous Ni-B spheres are amorphous. This method introduces a fraction of B into the Ni lattice, creating a disordered local structure around the Ni atoms. High-resolution transmission electron microscopy (HRTEM) [Figure 2C] indicates that there is no noticeable long-range atomic alignment because there are few clear domains with lattice fringes. Similarly, Cheng *et al.* achieved the transformation of Pd nanomaterials from a face-centered-cubic phase into an amorphous phase without destroying their
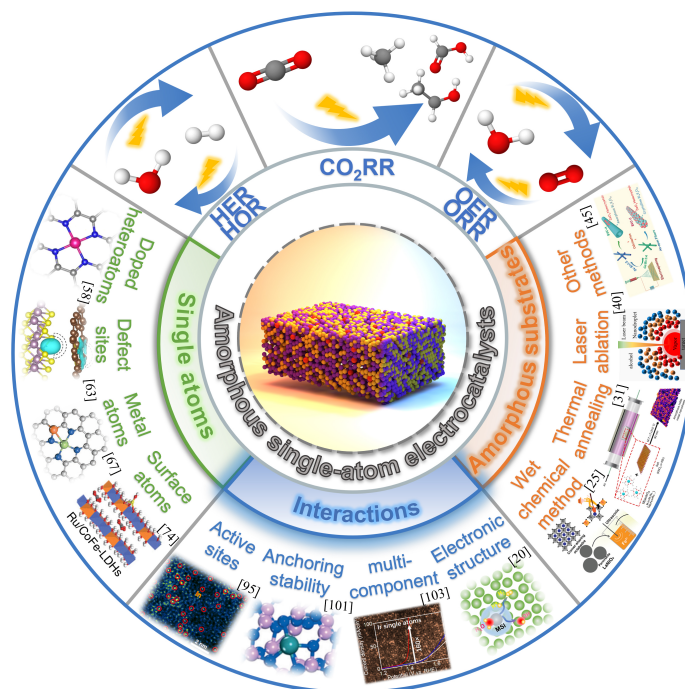
Figure 1. Schematic diagram of single-atom anchoring sites, synthesis strategies of amorphous substrates and interactions in the field of electrocatalysis.

integrity by simply mixing them with bismuth mercaptan I solution at room temperature[29]. Bismuth mercaptan I induced amorphization of outer Pd nanoparticle atoms, causing lattice expansion of inner atoms and eventual transformation into an amorphous phase. In another work, electrochemical lithiation of layered $Pd_3P_2S_8$ crystals yielded amorphous lithium-incorporated palladium phosphosulfide nanodots with abundant vacancies[30]. The lithium treatment deformed the Pd-S shell and reduced structural uniformity, introducing sulfur vacancies and Li doping. These amorphous nanodots exhibited excellent HER properties in acidic solutions due to their unique structure and high electrical conductivity.

Thermal annealing
Thermal annealing is a prevalent method for synthesizing amorphous materials, encompassing processes such as thermal reduction, oxidation, and phosphating. This approach is suitable for large-scale production and exhibits a degree of industrial feasibility. However, its implementation is costly due to the requirement for high-temperature equipment and precise atmosphere control. During appropriate thermal annealing, atomic diffusion and rearrangement lead to the formation of an amorphous phase.

In the thermal annealing process, parameters such as temperature, atmosphere, and annealing time significantly influence amorphous form formation. At low temperatures, partial phase transitions yield a composite of metal oxides and amorphous metals. Conversely, crystalline metals form at high temperatures, indicating a transition from an amorphous to a crystalline structure. For instance, in the work of Wu *et al.*, amorphous nanosheets must be annealed between the melt points of the metal acetylacetonate and the alkali salt[31]. Annealing at temperatures above the melt point of the alkali salt results in crystalline material formation, while temperatures below the metal acetylacetone melt point fail to drive the reaction. In practical applications, thermal reduction techniques are often combined with inert gases and high temperatures. For example, amorphous Li_3VO_4 anodes are synthesized via high-temperature annealing in
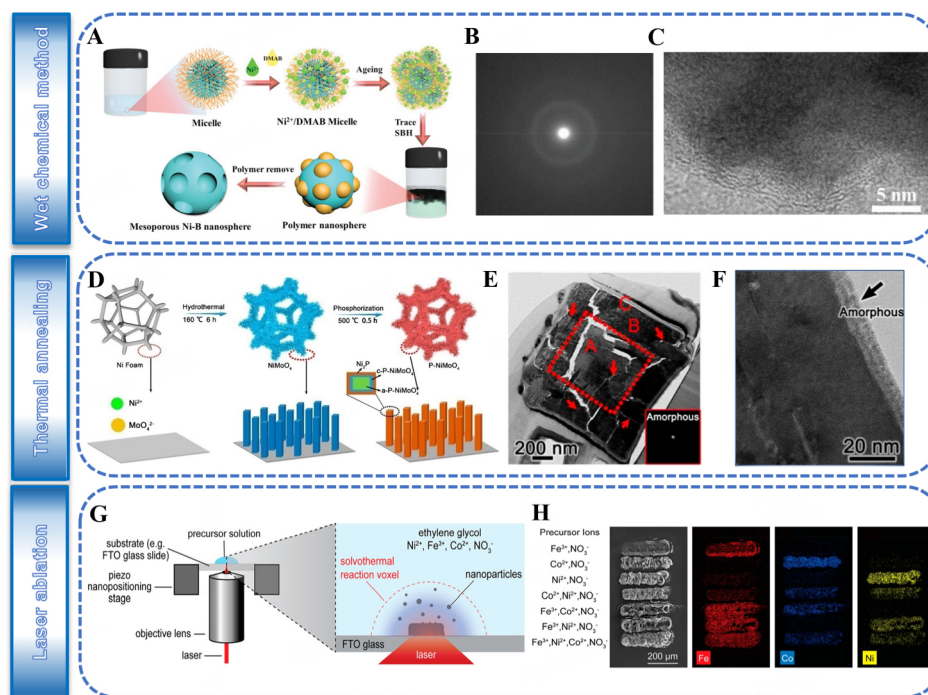
Figure 2. Various amorphous alloys prepared by different methods and structural characterization results of the amorphous alloys. (A) Mesoporous Ni-B nanospheres obtained from a dual chemical reduction. (B) SAED pattern of a single mesoporous Ni-B alloy sphere. (C) HRTEM images of 3D mesoporous Ni-B nanostructures. Reproduced with permission from Ref.[28] Copyright 2020, Wiley-VCH. (D) The synthesis process of P-NiMoO$_4$ nanoarrays via hydrothermal reaction and phosphorization process. (E) TEM specimen prepared by FIB lift-out techniques from P-NiMoO$_4$ nanorod. The inset shows the electron diffraction pattern of region A. (F) The magnified TEM image of region C in panel (E). Reproduced with permission from Ref.[35] Copyright 2024, American Chemical Society. (G) LITV method used to synthesize and direct-write mixed metal oxides from fluid precursors. (H) SEM images and SEM-EDS maps of single, binary, and ternary metal oxides and mixed metal oxides of Fe, Co, and Ni as prepared from solutions containing the ions listed at left. Reproduced with permission from Ref.[41] Copyright 2021, American Chemical Society.

vacuum, leading to surface oxygen escape and reduction of V^{5+} to V^{4+}[32]. This results in structural rearrangement, increasing lattice stress and decreasing oxygen vacancy, leading to gradual amorphization of the material. Additionally, the right reaction time is crucial for the manufacture of pure amorphous materials[33].

In thermal oxidation, a high-temperature oxygen atmosphere is employed to expose the substrate material to oxygen, facilitating a chemical reaction between oxygen molecules and the substrate surface. This process induces lattice deformation and distortion through oxidation reactions and atomic diffusion, thereby resulting in the amorphization of the material. Serrapede *et al.* demonstrated that amorphous TiO$_2$ formed at low temperatures, while anatase TiO$_2$ formed at high temperatures, suggesting that the oxidation temperature needs to be adjusted to obtain an ideal amorphous structural material[34].

Using a simple phosphating strategy, the interface between amorphous and crystalline phases and dislocation defects can be introduced into the catalyst. For instance, Zhang *et al.* synthesized a self-supporting electrocatalyst [Figure 2D], P-NiMoO$_4$, featuring a dislocation-rich structure comprising an amorphous Ni$_2$P/crystalline P-doped NiMoO$_4$/amorphous P-doped NiMoO$_4$ sandwich structure through thermal phosphidation strategies[35]. The phosphating process induces numerous edge and screw dislocations, prompting electron transfer from Ni and Mo ions to neighboring O and P atoms. Figure 2E gives a cross-sectional view of P-NiMoO$_4$ nanorods prepared by a focused-ion-beam lift-out technique,

indicating that the P-NiMoO$_4$ nanorods are composed of the amorphous-crystalline-amorphous sandwiched structure. The HRTEM image [Figure 2F] confirms that the outer shell of the nanorod is also amorphous. The heterogeneous interface effect between crystalline and amorphous phases modulates the electronic structure of electrocatalysts, enhancing catalytic activity in alkaline water and seawater.

Laser ablation
Femtosecond lasers, characterized by ultrashort pulse durations and ultrahigh peak power density, possess unique attributes such as nonlinear, non-equilibrium, and non-thermal processing capabilities[36-38]. Laser synthesis offers a cost-effective, time-saving, contactless, maskless, and environmentally friendly approach for producing various nanomaterials. Laser ablation is well-suited for low-volume production due to the sophisticated nature of the laser processing equipment.

The characteristics of the laser can induce transient heating in processing solutions during the reaction, potentially introducing vacancies or generating defect sites, leading to material amorphization. In the work of Zhao *et al.*, CoS$_x$ nanospheres anchored to carbon fiber cloths were found to provide more active sites due to the presence of sulfur vacancies caused by a high-pressure field induced by laser processing, enhancing HER and nitrogen reduction reaction (NRR) activity[39]. Upon cessation of laser irradiation, the large temperature gradient induced by local heating alters the kinetics of phase transitions, affecting the phase transition pathways and rates of crystalline structures. Rapid cooling of localized high-temperature regions often results in a delay in phase transitions of crystal structures. Structures fail to rearrange into stable crystalline phases within a sufficient timeframe. The inability of crystal structures to undergo complete rearrangement and relaxation in a timely manner leads to the formation and diffusion of lattice defects. These factors collectively contribute to the synthesis of non-crystalline phases via laser irradiation. Liu *et al.* stated that when the laser interacts with a solid target, plasma is generated in the gas phase[40]. At the interface of the cool liquid and laser-induced plasma, a chemical reaction occurs, leading to the condensation of atoms in the liquid and the formation of small amorphous nanoparticles[40]. Additionally, As shown in Figure 2G, McGee *et al.* synthesized metastable and mixed transition metal oxide materials directly from solution precursors using a simple laser-induced thermal voxel method[41]. The resultant materials deposited from the single, binary, and ternary combinations of precursors were analyzed with scanning electron microscopy (SEM) and energy dispersive X-ray spectroscopy [Figure 2H]. This laser processing method enhanced catalytic activity by generating distorted active sites at the interface between crystal nanoparticles and amorphous substrates, thus reducing overpotential and improving OER performance[41].

Adjusting laser parameters can enhance hybrid microstrain and lattice strain, introducing structural irregularities and local defects[42]. Li *et al.* utilize instantaneously formed femtosecond laser double pulse sequences to maximize the proportion of Mo^V defective substances, thus improving catalytic activity[43]. Budiyanto *et al.* conducted molecular dynamics simulations of the Co$_3$O$_4$/water interface at different temperatures[44]. They revealed stronger interactions between the reconstructed Co$_3$O$_4$(001) surface and water/hydroxide molecules, resulting in more Co^{2+} pushing up from the surface into the tetrahedral coordination. The formation of amorphous cobalt hydroxide precursors potentially plays a crucial role in the formation of active sites during OER.

Others
In addition to the methods mentioned above, there are many ways to synthesize amorphous materials, such as electrochemical synthesis, electrospinning process[45], reactive magnetron sputtering deposition and physical approaches.

Reactive magnetron sputtering deposition allows for highly controllable catalyst morphology and composition by adjusting deposition parameters and target materials. However, this method requires specialized equipment and conditions, resulting in higher costs. At room temperature, reactive magnetron sputtering deposition increases the number of crystal defects and sulfur defects of MoS_x, leading to the discovery of coordinated unsaturated Mo atoms at the edge of the S-Mo-S layer. These crystal defects and sulfur defects produce coordination-unsaturated atoms. A reaction mechanism using Mo atoms with overhanging bonds as the catalytic active site was proposed by Xi *et al.*[46].

In physical methods of synthesis, chemical reactions are not involved, which helps maintain the purity and stability of the catalyst. However, for certain complex catalyst structures, physical methods may be infeasible. For the physical strategy, the mechanism of amorphization is that the crystal lattice will be broken by the application of external stresses (e.g., mechanical force, irradiation, and heat). Therefore, the material will no longer have a long-range order, but a short-range order of amorphous. High pressures and mechanical processes cause the crystal structure to collapse to form an amorphous structure[47,48]. Low-temperature irradiation such as X-ray photooxidation and microwave-induced thermal agitation also produce amorphous processes[49-51].

Anchoring sites of single-atom
While various methods can be employed to anchor single atoms onto different amorphous substrates, a significant challenge persists: the high surface energy of loaded single atoms often leads to their agglomeration, forming nanoclusters and nanoparticles during catalysis. To address this issue and design stable single-atom electrocatalysts, a comprehensive understanding of the interaction between anchoring position and single atoms is imperative. Anchoring positions for single atoms primarily include heteroatoms, defects, and metal atoms within the substrate. Therefore, in the subsequent chapters, we will systematically outline the anchoring mechanisms of single atoms on various types of anchoring sites, including heteroatoms, defects, metal atoms, and others present in the substrate. Additionally, we will highlight some of the advantages offered by amorphous substrates in facilitating the anchoring of single atoms.

Doped heteroatoms
Heteroatoms, such as N, O, S, and P, are commonly employed for anchoring single atoms in catalysis[52]. Carbon-based materials such as graphene, featuring atomically dispersed $TM-N_x$ sites, offer a promising alternative to noble metal oxygen reduction catalysts. These catalysts typically coordinate metal single-atom sites with heteroatoms through pyrolysis, providing a flexible and adjustable coordination environment. This approach enables fine-tuning of single-atom charge density, leading to significant advancements in single[53] and multi-heteroatom doping[54,55] and multi-metal active sites[56-58]. For instance, Zhao *et al.* employed a misplaced deposition strategy to anchor Co atoms with nitrogen[58], resulting in the formation of Dual-Metal Hetero-Single-Atoms [Figure 3A]. X-ray absorption fine structure (XAFS) analysis revealed that Co coordinated with four nitrogen atoms, forming CoN_4 sites [Figure 3B and C]. This active site was incorporated into CuC_4@HC, leading to a significantly polarized surface charge distribution [Figure 3D] and enhanced catalytic activity for HER.

Defect sites
When employing defect engineering to design SACs, the defect structure on the substrate serves to capture single atoms and stabilize them through charge transfer between defects and single atoms. Therefore, under-coordinated anionic defects[59,60] and cationic defects[61,62] in the catalytic material can serve as anchor sites for single atoms. S and O vacancies are common anionic defects used in single-atom anchoring.
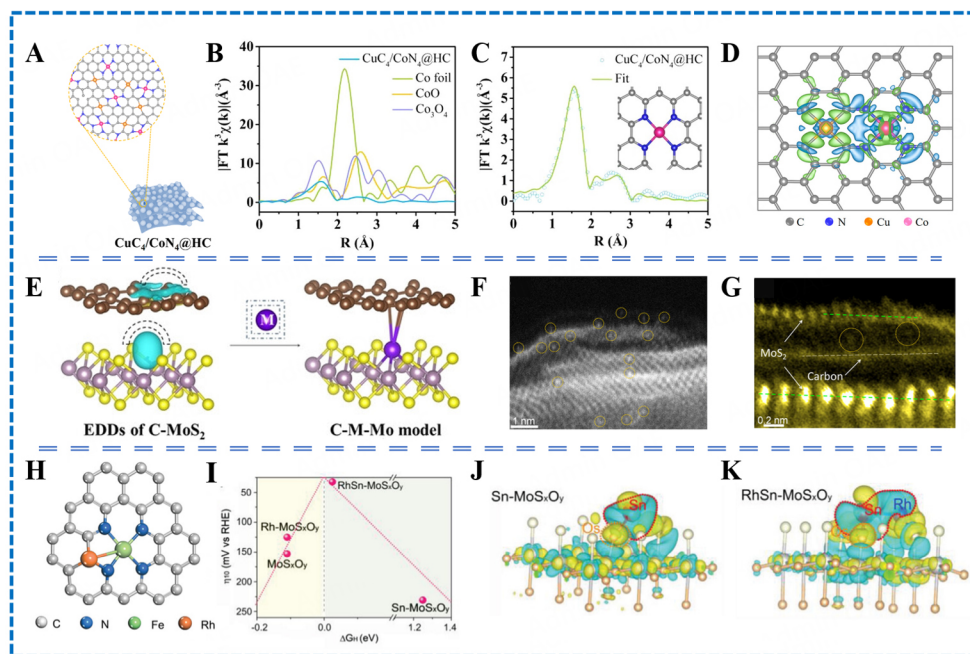
Figure 3. Single atoms are anchored at doped heteroatoms(A-D), defect sites(E-G) and metal atoms(H-K): (A) anchoring diagram of $CuC_4/CoN_4@HC$. (B) FT k^3-weighted EXAFS spectra for the Co K-edge of $CuC_4/CoN_4@HC$, Co foil, CoO, and Co_3O_4. (C) Model of CoN_4 sites and fitting curves of $CuC_4/CoN_4@HC$. (D) Top view of the differential charge densities of $CuC_4/CoN_4@HC$. Reproduced with permission from Ref.[58] Copyright 2021, American Chemical Society. (E) The electron density differences in the C-MoS_2, the structure model of C-M-Mo. (F and G) AC TEM images of C-Co-MoS_2. Reproduced with permission from Ref.[63] Copyright 2023, Wiley-VCH. (H) The model structure of Fe-Rh interbonds. Reproduced with permission from Ref.[67] Copyright 2020, Wiley-VCH. (I) Plot of the H adsorption free energy versus η_{10}. (J and K) The differential charge densities of $Sn-MoS_xO_y$ (J), $RhSn-MoS_xO_y$ (K). Reproduced with permission from Ref.[68] Copyright 2022, Wiley-VCH.

Gong *et al.* employed density functional theory (DFT) calculations to guide the design of single atoms anchored at S vacancies[63]. Their calculations revealed that MoS_2 induces an electron deficiency of 0.2 |e| at the sulfur vacancy, forming an "E-Lock" mechanism capable of capturing metal atoms and anchoring them *in situ*, as depicted in the accompanying Figure 3E. High-angle annular dark-field (HAADF) images [Figure 3F and G] obtained via aberration-corrected transmission electron microscopy (AC-TEM) further corroborated the successful preparation of Co single atom structures anchored by the "E-Lock". Electrochemical tests confirmed the stable hydrogen evolution performance of catalysts. Indeed, numerous reports utilize cation defects in materials as anchor sites for single atoms. These cationic defects provide locations where single atoms can bind and remain stabilized, contributing to enhanced catalytic performance. For example, Elbakkay *et al.* successfully anchored highly loaded Cu single atoms utilizing cationic vacancies in CoFe-layered double hydroxides, achieving stable and efficient OER[64].

Compared to crystalline substrates, amorphous substrates offer significant advantages for anchoring single atoms due to their abundance of intrinsic defects. Zhang *et al.* demonstrated this by anchoring single Pt atoms and clusters in amorphous $Fe_5Ni_4S_8$[65]. The presence of numerous defects in the substrate facilitated the capture of highly active single atoms. This resulted in efficient catalytic performance, with overpotentials of 30 mV under acidic conditions, 65 mV under alkaline conditions, and 98 mV under neutral conditions at a current density of 10 mA cm⁻².

Metal atoms
Single atoms can be anchored by forming metal-metal (M-M) bonds with adjacent metal atoms. Metal atoms can serve as anchor sites for another single metal atom loaded onto the substrate. This approach has been reported in several studies and offers a unique strategy for anchoring single atoms on various substrates. Wang *et al.* demonstrated this method by introducing Pt atoms onto the surface of commercial CeO_2, utilizing them to anchor inert Fe atoms nearby[66]. Their results revealed electron transfer between Fe and Pt, with the presence of adjacent Fe atoms reducing the electron density of Pt, thereby activating reverse water-gas shift reaction performance. Our group's related research also employed M-M bonds to anchor a series of single atoms. For instance, we converted Fe nanoparticles at low temperatures through Fe-Rh interbonds [Figure 3H], resulting in FeRh dual-atom catalysts supported on nitrogen-doped hollow carbon spheres[67]. This catalyst exhibited superior HER performance. Amorphous materials, characterized by short-range ordered structures, offer highly exposed surfaces conducive to metal atom proximity and active site exposure. Hence, we synthesized a Rh-Sn coordinated high-efficiency HER catalyst on an amorphous molybdenum oxysulfide substrate[68]. Calculation results revealed a synergistic effect between Rh and Sn, where Rh transferred the attack site of H to Rh through electron interaction with Sn and apical S, thereby altering hydrogen adsorption strength and achieving low overpotential HER [Figure 3I-K].

Anchoring single atoms can also involve utilizing a metal array. Evenly distributing single atoms on the metal array to create a single-atom alloy structure serves as an efficient anchoring method. This approach is widely adopted, and recent studies[69-73] have focused on synthesizing single-atom alloys through M-M bonds and applying them across various fields.

Others
In addition to the above anchoring mechanisms, single atoms can also be anchored by bonding with non-metallic atoms on the surface of the material[60,74,75] or by utilizing specific substrates to constrain their spatial arrangement[76]. For instance, Jiang *et al.* demonstrated the assembly of Ni and Fe single atoms within the interlayer of MoS_2[77]. This interlayer constraint structure provides protection to single atoms while enhancing the overall water splitting activity. Moreover, when the confinement occurs at the interface between crystal and amorphous materials, it can promote the formation of heterogeneous interfaces and the introduction of single atoms simultaneously, further enhancing the catalytic performance of the catalyst. For example, Xi *et al.* synthesized Pd SACs dispersed at the interface of graphene oxide and amorphous carbon[78]. By loading single-atom Pd on the constrained interface, they achieved catalysts with exceptionally high activity and stability.

Characterization techniques of amorphous single-atom catalyst
The characterization techniques for crystalline SACs have been extensively reported[79-81]. However, the complex composition of amorphous substrates poses significant challenges for accurate characterization. Therefore, summarizing the characterization methods for amorphous SACs is essential.

X-ray diffraction (XRD) is a widely used characterization method. The spacing between crystals is generally close to the wavelength of X-rays, so when the material is irradiated by X-rays, diffraction occurs. The superposition of diffraction waves strengthens or weakens the rays in certain directions, allowing the analysis of the crystal structure based on diffraction results at different angles. Crystalline materials have a long-range order with atoms arranged periodically, resulting in clear diffraction peaks. In contrast, amorphous materials lack a periodic structure and exhibit a broad peak at a lower diffraction angle, which is a key indicator of an amorphous structure. Conventional XRD analysis cannot accurately characterize amorphous materials. However, it is feasible to analyze the short-range ordered structure using the Pair

Distribution Function (PDF). The PDF can be obtained through the Fourier transform of the scattering pattern[82]. The intensity of the diffuse scattering may be related to the short-range structure of the material. For amorphous materials, the measured PDF typically represents the average of all variations. This information can be processed using modeling methods to determine the possible distribution of structural properties within the material.

Transmission electron microscopy (TEM) serves as a crucial tool in the field of electrocatalysis for examining the microstructure of materials. By irradiating the sample with an electron beam, TEM enables the acquisition of high-resolution images through the analysis of phase and interference information transmitted by electrons. TEM proves adept at identifying amorphous materials by analyzing diffraction patterns, density distributions, atomic alignment, and high-resolution microscope images. Due to the disordered atomic arrangement of amorphous materials, it is common for TEM diffraction patterns to exhibit continuous annular or diffuse spots instead of clear lattice diffraction points. These irregular diffraction spots reflect the disorder and short-range order inherent in amorphous materials. The density distribution observed in TEM images of amorphous samples typically exhibits homogeneity or irregularity. In contrast to crystals, where atoms exhibit significant periodicity, amorphous materials lack a well-defined periodic structure in their density distribution due to the absence of ordered atomic arrangements. Furthermore, in high-resolution TEM images, the atomic arrangement of amorphous samples tends to appear random or irregular. Although localized order may be present to some extent, the overall atomic arrangement remains disordered and defies description through lattice constants or identifiable lattice points.

In addition to the commonly used methods mentioned above, several techniques have been employed to describe the precise structure of amorphous substrates[21]. Raman spectroscopy, scanning TEM (STEM), nanobeam electron diffraction (NBED), and XAFS are utilized to reveal the true geometric structure of amorphous catalysts. These methods provide a foundation for the accurate characterization of amorphous SACs.

CHARACTERISTICS AND MECHANISM

The design of efficient electrocatalysts has become an important part of the exploration of sustainable energy technology. A comprehensive understanding of the structure-activity relationship and reaction mechanisms is crucial for designing rational and efficient catalysts. The structure-function relationship of amorphous materials and the significance of the structure of anchored single atoms on amorphous materials in specific catalysis are elucidated from the perspective of physical properties and catalytic mechanisms.

Physical characteristics

The distinct physical properties of amorphous materials profoundly influence electrocatalysis performance, underscoring the importance of comprehending the internal relationship between these properties and electrocatalytic reaction mechanisms. Amorphous materials typically exhibit a larger specific surface area compared to other materials, providing an expanded reaction space and more pore structure conducive to catalytic reactions. This loose and porous structure facilitates the diffusion of reactants and products between catalytically active sites, thereby enhancing mass transfer in the electrocatalytic process and improving reaction kinetics.

The inherent complexity of amorphous materials enables a more flexible and easily adjustable composition, allowing for the regulation of adsorption and desorption strengths of reactant molecules on the material

surface. By manipulating specific components within the material, specific reaction pathways can be promoted, reaction intermediates can be stabilized, and catalytic activity can be enhanced. The abundant dangling bonds and coordination unsaturated atoms of amorphous materials are also related to their own flexible composition, so that the active sites can be better exposed from the bulk phase, rather than the crystal can only be exposed from the surface. Klingan *et al.* observed that the turnover frequency of Co active sites in the bulk phase of amorphous materials closely resembles that of surface activity, leading to their proposition that the OER activity of amorphous bulk materials is more aptly described by volume activity[83].

Moreover, the degree of disorder in materials often correlates with their electrical properties, where microscopic disordered structures can influence macroscopic electrical properties. Tian *et al.* synthesized two-dimensional (2D) amorphous carbon at varying temperatures to investigate the impact of structural disorder on material properties[84]. Utilizing a 2D system simplified complexity, allowing for a closer examination of structural issues. Atomic-resolution electron microscopy revealed the presence or absence of medium-range order and temperature-dependent densities of nanocrystallites, serving as proposed order parameters to comprehensively describe disorder and correlate microstructure with macroscopic electrical properties. Since electron conduction is integral to the electrocatalytic process, the influence of micro-disordered structure on the conductivity of amorphous materials can affect efficient electron conduction and subsequently influence catalytic processes. In 2018, Su *et al.* observed continuous improvement in the catalytic performance of Ni-Fe Prussian blue analogs, accompanied by the formation of an amorphous phase during the OER[85]. Theoretical calculations suggested that the formation of the amorphous phase increased the component of O 2p near the Fermi level and reduced the band gap, promoting improvements in kinetics.

Reaction mechanisms

Amorphous materials can adsorb multiple reactant molecules simultaneously, thereby facilitating catalytic reactions. The absence of long-range ordered structure leads to the presence of numerous defects and active sites on their surfaces, promoting the adsorption of reactant molecules. Duan *et al.* observed that amorphous NiFeMo oxides synthesized exhibited a more rapid surface self-rebuilding process compared to crystals[86]. This rapid evolution led to a significant loss of Mo cations, as depicted in Figure 4A and B, resulting in the generation of abundant oxygen vacancies. Further insights were obtained through DFT calculations aimed at elucidating the role of oxygen vacancies in facilitating the OER process. As shown in Figure 4C, the presence of oxygen vacancies in the structure decreased the ΔG_{H^*} value associated with the release of O_2 by *OOH intermediates at the Fe site. These findings suggest that such vacancies promote weak *OOH adsorption, thereby enhancing the OER activity. Numerous experimental and theoretical studies have demonstrated that the surface reaction proceeds through the initial activation of the CO_2 molecule, followed by the conversion of the intermediate *CO to subsequent hydrogenated species via proton-electron transfer. Figure 4D illustrates the CO_2RR process facilitated by high-altitude InO_x nanorods (H-InO_x NRs), as prepared by Zhang *et al.* via a straightforward heat treatment method[87]. CO_2 molecules undergo vigorous adsorption and activation upon interaction with H-InO_x NRs, facilitated by the introduction of oxygen vacancies. Simultaneously, electrons generated by the oxygen vacancies facilitate charge transfer in subsequent reactions. Consequently, the combination of strong adsorption, effective activation, and efficient charge transfer mechanisms contributes to the favorable selectivity observed in CO_2RR.

When a single atom lacks surrounding atoms, its surface reactivity increases, facilitating effective adsorption of reactant molecules. This adsorption capacity enhances interaction with the catalyst surface, thereby boosting the reaction rate[88]. Zhang *et al.* discovered that C_{60}-modified Pt single-atom sites enhance water
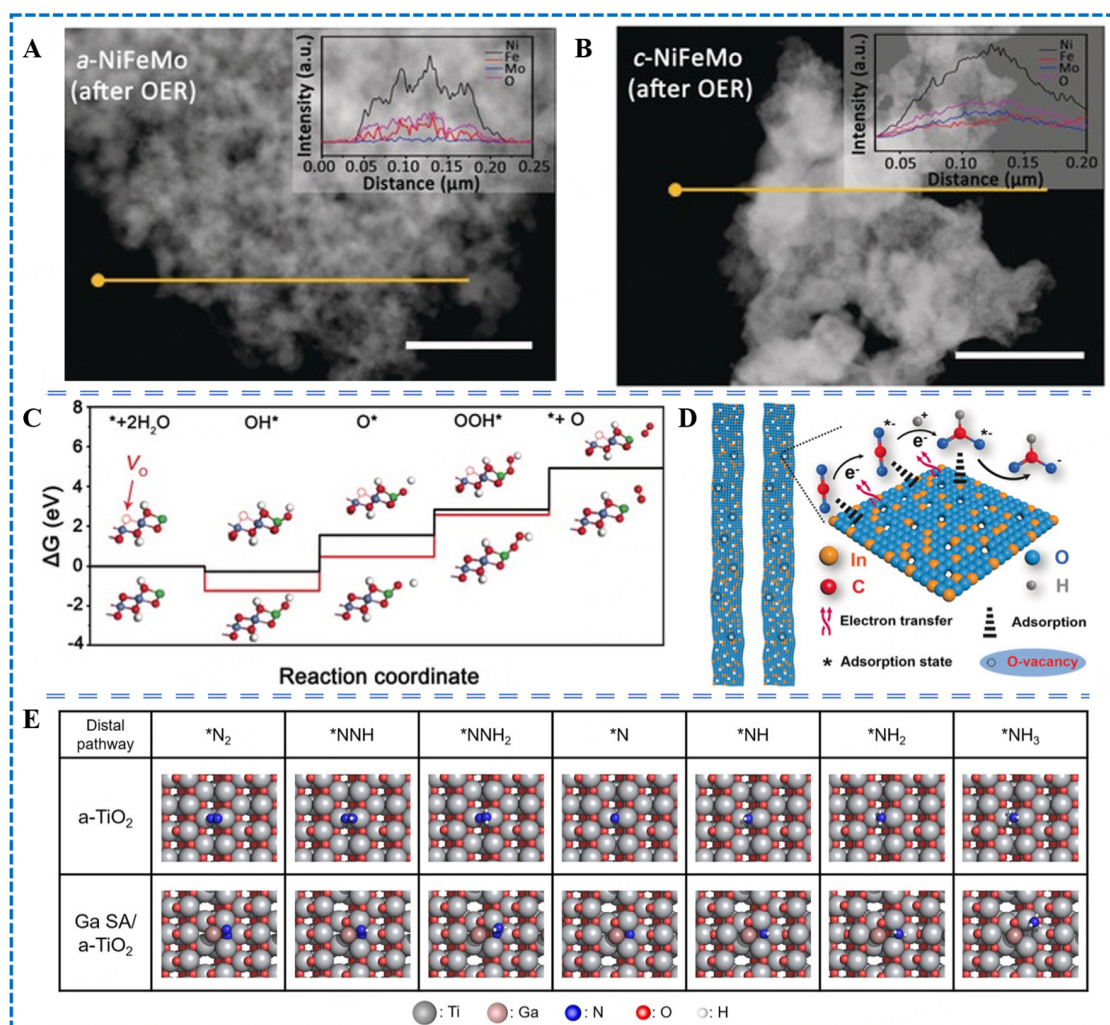
Figure 4. The impact of amorphous materials and synergistic monoatomic components on enhancing substance adsorption. STEM images of a-NiFeMo (A) and c-NiFeMo (B) after OER, respectively. Insets in (A and B) show corresponding EDX line scan profiles. (C) ΔG_{H^*} change diagrams of the OER reduction reaction on the NiFe-OOH surface models with (black line) and without (red line) O-vacancies. Reproduced with permission from Ref.[86] Copyright 2019, Wiley-VCH. (D) The scheme of the CO_2RR processes in InO_x NRs. Reproduced with permission from Ref.[87] Copyright 2019, Wiley-VCH. (E) Optimized structures of the intermediates for N_2 adsorption and reduction on a-TiO$_2$ and Ga SA/a-TiO$_2$ surfaces. Reproduced with permission from Ref.[92] Copyright 2022, American Chemical Society.

adsorption and hydrogen desorption, representing the optimal active sites within Pt/C$_{60}$[89]. Numerous Single-Atom Catalysts have demonstrated remarkable selectivity towards the reduction of CO_2 over the competing HER. This preference is attributed to the favorable adsorption of carboxyl (*COOH) or formate (*OCHO) intermediates over hydrogen (*H) on these catalysts[90]. Cheng *et al.* noted that Pt single atoms supported on nitrogen-doped graphene nanosheets acquire a positive charge[91]. During the reaction, two hydrogen atoms bond to the Pt. Bader charge analysis reveals a significant overlap between Pt 5d and H 1s orbitals, generating numerous new states beyond the Fermi level. This indicates charge transfer from Pt to H during the pivotal proton reduction process.

Catalysts formed by anchoring single atoms onto amorphous materials offer several advantages over pure amorphous materials or SACs. Firstly, amorphous materials provide abundant active sites and surface

defects, facilitating the adsorption of intermediate molecules and promoting catalytic reactions. Secondly, anchoring single atoms enhances the stability of active sites, reducing the possibility of uncontrolled deactivation and thus extending the catalyst's lifespan. Additionally, the structure of amorphous materials typically exhibits higher surface area and porosity, facilitating the diffusion rate of intermediate molecules and thereby enhancing the rate and efficiency of catalytic reactions. Through the rational design of the interaction between single atoms and amorphous materials, precise control over the adsorption and desorption processes of substances can be achieved, thereby enhancing the performance and efficiency of catalysts. Zhang *et al.* discovered that amorphous TiO_2 nanofibers, as opposed to vacancy-engineered TiO_2 nanocrystals, possess abundant intrinsic oxygen vacancies and dangling bonds in nature[92]. Utilizing the confinement effect of oxygen vacancies, well-isolated Ga single atoms were successfully synthesized. These Ga single atoms promote the selective adsorption of N_2 on the catalyst surface, while oxygen vacancies facilitate the subsequent activation and reduction of N_2 [Figure 4E]. Chen *et al.* exploited the synergistic effect of strong binding and stabilization of single Pt atoms along with strong metal-support interaction between the *in situ* anchored Pt atoms and Fe_2O_3 to reduce CO adsorption[93]. Furthermore, the presence of distorted amorphous Fe_2O_3 with oxygen vacancies facilitates O_2 activation, thereby enhancing CO oxidation on nearby Pt sites or the interface between Pt and Fe_2O_3. This leads to an atomic catalyst with exceptionally high CO oxidation activity.

INTERACTIONS BETWEEN AMORPHOUS SUBSTRATES AND SINGLE ATOMS

The amorphous substrate presents numerous defects, unsaturated bonds, and dangling bonds, offering significant advantages in capturing single atoms to enhance active sites and prevent the agglomeration. Additionally, in contrast to crystals, amorphous substrates afford a more flexible coordination environment for single atoms, facilitating the synergistic activation of various sites and structures and the optimization of catalytic center electronic configurations. In order to further study the interaction between single atoms and amorphous substrates, the subsequent sections will primarily summarize and propose corresponding adjustment strategies from four perspectives: increasing active sites, preventing single-atom agglomeration, fostering multi-component collaboration, and optimizing electronic structure [Table 1]. It is important to note that while these classifications are not entirely mutually exclusive, detailed categorization is necessary for a better comprehension of the interaction between single atoms and amorphous substrates.

Increasing active sites

An increase in the density of single atoms anchored on suitable substrate materials can enhance the number of active sites for electrocatalytic reactions, thus leading to improved catalytic effects. However, achieving higher loading of single atoms necessitates the provision of a large number of anchoring sites by the substrate, which poses a significant challenge for crystalline materials.

Amorphous materials, lacking the long-range ordered structures found in crystalline materials, offer a large number of defects and unsaturated structures, facilitating the anchoring of single atoms with high content. For instance, during the co-precipitation process, the addition of F ions can promote the transformation of $Co(OH)_x$ to CoOOH, resulting in the formation of an amorphous structure with an edge surface[94]. HRTEM images demonstrate that the incorporation of F ions benefits the transformation of the structure, leading to the formation of a wider amorphous boundary [Figure 5A and B]. This wider boundary, rich in oxygen vacancies, provides numerous anchoring sites for Ir single atoms. HAADF-STEM images further confirm that the number of Ir single atoms anchored on the highly amorphous boundary is significantly larger [Figure 5C and D], showcasing the anchoring advantage of the amorphous substrate. Additionally, amorphous MoO_3 has proven to be an efficient substrate for high-density single-atom anchoring. Chen *et al.* utilized supercritical CO_2 to prepare In single atoms loaded on amorphous MoO_3 for NO

Table 1. Summary table of interaction mechanism

Electrocatalyst	Cooperative mode	Electrolyte	Application	Performance	Ref.
$Ir_1/CoOOH(F)$	Increasing active sites	1.0 M KOH	OER	η_{10} = 238 mV	[94]
$In_1/a\text{-}MoO_3$	Increasing active sites	0.5 M Na_2SO_4	NORR	NH_3 yield rate = 242.6 µmol h^{-1} cm^{-2} FE = 92.8%	[95]
$Pt_1/MoO_{3\text{-}x}$	Increasing active sites	0.5 M H_2SO_4	HER	η_{10} = 23.3 mV	[96]
$Pt\text{-}Fe_5Ni_4S_8$	Increasing active sites	0.5 M H_2SO_4	HER	η_{10} = 30 mV	[65]
		1.0 M KOH		η_{10} = 65 mV	
		1.0 M phosphate buffer solution (PBS)		η_{10} = 98 mV	
Ru $SAs\text{-}MoO_{3\text{-}x}/NF$	Increasing active sites	1.0 M KOH	OER	η_{10} = 209 mV	[98]
		1.0 M KOH	HER	η_{10} = 36 mV	
		1 M KOH seawater	OER	η_{100} = 539 mV	
$h\text{-}Pt_1\text{-}CuS_x$	Increasing active sites	O_2-saturated 0.5 M $HClO_4$	ORR	H_2O_2 productivity = 546 ± 30 mol kg_{cat}^{-1} h^{-1} FE = 92%-96%	[97]
PBN-300-Ir	Preventing agglomeration	0.5 M H_2SO_4	HER	η_{10} = 17 mV	[99]
$SA\text{-}Pt/WO_3$	Preventing agglomeration	0.1 M KOH	ORR	/	[100]
Ru SAs@PN	Preventing agglomeration	0.5 M H_2SO_4	HER	η_{10} = 24 mV	[101]
Rh-SACs/HNCR	Preventing agglomeration	N_2-saturated 0.5 M H_2SO_4 + 0.5 M HCOOH	FAOR	j_p/j_n = 2.10	[102]
$IrCoO_x$ ANSs	Multi-component collaboration	1.0 M KOH	OER	η_{10} = 152 ± 5.2 mV	[103]
$NiFeIr_x/Ni$ NW@NSs	Multi-component collaboration	1.0 M KOH	OER	η_{10} = 200 mV η_{100} = 250 mV	[104]
Pt/NiRu-OH	Multi-component collaboration	1.0 M KOH	HER	η_{10} = 38 mV	[105]
Fe/SAs@Mo-based-HNSs	Multi-component collaboration	1.0 M KOH	HER	η_{10} = 38.5 mV	[106]
$Fe_1\text{-}N\text{-}NG/RGO$	Multi-component collaboration	O_2 saturated 0.1 M $HClO_4$	ORR	$E_{1/2}$ = 0.84 V	[107]
Pt/TiB_xO_y	Optimizing electronic structure	H_2-saturated 0.5 M H_2SO_4	HER	Mass activity = 37.8 A mg_{Pt}^{-1} η = 50 mV	[109]
$Pt\text{-}SA/a\text{-}MoO_x$	Optimizing electronic structure	0.5 M H_2SO_4	HER	η_{10} = 19 mV	[110]
Ru SAs/AC-FeCoNi	Optimizing electronic structure	O_2-saturated 1 M KOH solutions	OER	η_{10} = 205 mV	[111]
Ru-a-CoNi	Optimizing electronic structure	1.0 M KOH	HER	η_{10} = 15 mV	[20]
amorphous Fe-ZrP	Optimizing electronic structure	1.0 M KOH	OER	η_{10} = 209 mV	[112]
$Sb_1/a\text{-}MoO_3$	Optimizing electronic structure	NO saturated 0.5 M Na_2SO_4	NORR	NH_3 yield rate = 273.5 µmol h^{-1} cm^{-2} FE = 91.7%	[113]

reduction to NH_3 [Figure 5E and F][95]. HAADF-STEM images reveal a uniform dispersion of a large number of In single atoms on amorphous MoO_3. Test results demonstrate that the content of In single atoms reaches 8.2 wt%, significantly higher than that reported in the literature for single atoms on carbon-based substrates. Liu *et al.* also achieved high content of single-atom loading using amorphous MoO_3, leveraging the strong interaction between Pt atoms and defect substrates to anchor single-atom Pt atoms on the defects of the substrate, resulting in a final loading of 4.1 wt%[96]. The catalyst exhibits HER performance that exceeds that of commercial Pt/C. Furthermore, Shen *et al.* employed amorphous materials as the substrate for anchoring single-atom Pt with high content, constructing amorphous CuS_x hollow nanospheres with a content of up to 24.8 at% Pt single atoms[97]. Results indicate good two-electron oxygen reduction performance of the catalyst. The aforementioned examples highlight that defects in amorphous substrates facilitate the anchoring of more single atoms and provide additional active sites for electrochemical reactions, enabling the possibility of high-density loading of single atoms.

Moreover, compared with crystalline materials, amorphous materials with more defects can also serve as additional active sites for synergistic single-atom catalysis. For example, Feng *et al.* combined Ru single atoms with amorphous MoO_3 substrates to achieve low-energy water splitting[98]. The presence of numerous oxygen vacancies on the amorphous substrate enables the uniform dispersion and anchoring of Ru single atoms. Electrochemical tests reveal that the amorphous SAC exhibits a larger electrochemical active surface area than the crystal SAC, providing more active sites for the reaction. Additionally, Zhang *et al.* anchored a single Pt atom and cluster in $Fe_5Ni_4S_8$, observing that as the ball milling time increased, the defects in $Fe_5Ni_4S_8$ also increased[65]. Substrates with more defects can provide more active sites for HER and more anchoring sites for Pt atoms. The prepared amorphous SAC exhibits excellent HER performance under acidic, alkaline, and neutral conditions. Therefore, utilizing an amorphous substrate to increase defects, promote high-density single-atom anchoring, and enhance additional active sites represents a highly feasible strategy.

Preventing agglomeration

The defects in the amorphous substrate not only provide a large number of active sites, but also promote the stronger anchoring of single atoms, thereby preventing the occurrence of agglomeration. Inspired by the trapping of single atoms via nanometer defects through C-C bond reconstruction, Liu *et al.* synthesized a series of amorphous carbon-supported SACs. These catalysts feature a self-healing 2D conjugated carbon framework and C-M bond, augmenting the stability of single atoms[99]. Zhang *et al.* prepared Pt SAC (SA-Pt/WO$_3$) dispersed on the surface of WO_3 amorphous tungstenic acid[100]. Differential scanning calorimetry and H_2 temperature-programmed reduction results, as depicted in Figure 5G and H, indicated that SA-Pt/WO$_3$ exhibited the highest endothermic temperature and reduction temperature, suggesting the strongest interaction between Pt single atoms and the substrate. This strong interaction ensures the high dispersion of Pt single atoms during catalytic processes. Yang *et al.* anchored Ru single atoms on the P vacancy of amorphous phosphorus nitride imide nanotubes[101]. The presence of numerous dangling unsaturated P vacancies stabilized Ru single atoms, as evidenced by the catalytic performance remaining largely unchanged after 24 h of continuous operation at a current density of 163 mA cm^{-2} in an acidic medium, underscoring the role of amorphous substrates in preventing agglomeration.

Moreover, amorphous substrates can utilize spatial constraints to achieve stronger anchoring of single atoms. For instance, Xi *et al.* initially employed theoretical calculations to predict that the graphene/amorphous carbon structure could form a stronger bond with Pd[78]. Subsequently, they synthesized Pd SACs dispersed at the interface between graphene oxide and amorphous carbon based on theoretical guidance. Hu *et al.* utilized the hollow structure and effective carbon confinement of carbon nanorods to constrain Rh single atoms[102]. Test results demonstrated that no CO oxidation current was detected in the
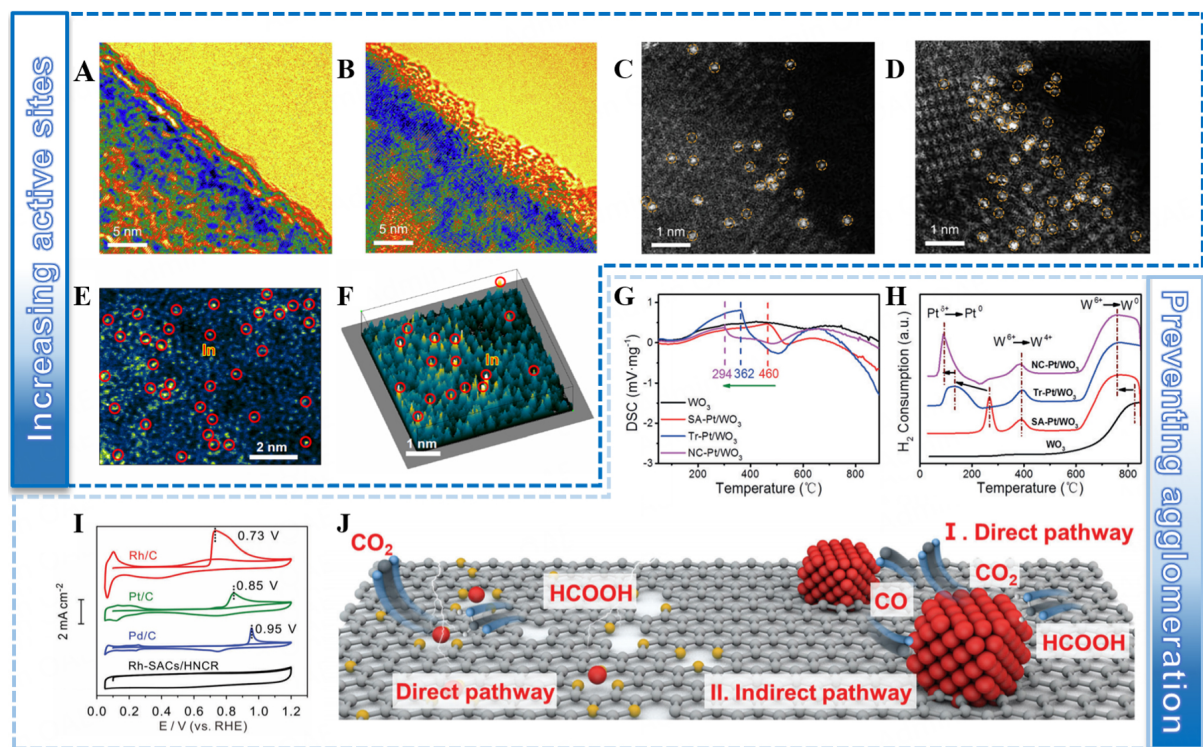
Figure 5. The amorphous substrates to increase active sites and prevent the agglomeration of single atoms: (A) HRTEM image of $Ir_1/CoOOH$. (B) HRTEM image of $Ir_1/CoOOH$ (F). (C) HAADF-STEM image of $Ir_1/CoOOH$. (D) HAADF-STEM image of $Ir_1/CoOOH$ (F). Reproduced with permission from Ref.[94] Copyright 2023, Elsevier. (E) AC-HAADF STEM image and corresponding of In_1/a-MoO_3. (F) 3D intensity profile of In_1/a-MoO_3. Reproduced with permission from Ref.[95] Copyright 2023, RSC. (G) DSC, (H) H_2-TPR curves of bare WO_3 and Pt/WO_3 hybrids. Reproduced with permission from Ref.[100] Copyright 2018, Wiley-VCH. (I) CO stripping curves of Rh/C, Pt/C, Pd/C and Rh-SACs/HNCR. (J) Schematic diagram of the possible FAOR pathway for Rh-SACs/HNCR and Rh/C. Reproduced with permission from Ref.[102] Copyright 2022, Wiley-VCH.

CO stripping curves [Figure 5I], indicating the construction of a solid single-atom site and thereby circumventing the co-conformation dehydration pathway in the electrooxidation of formic acid [Figure 5J].

Multi-component synergy

The catalytic effect of an electrocatalyst can be adjusted by altering the chemical state of the electrode surface, the atomic arrangement structure, and other factors. Several studies have demonstrated that the amorphous substrate facilitates changes in the chemical state of the electrode surface and enables multi-site synergistic catalysis. For instance, amorphous CoO_x nanosheets, with their large surface area and high chemical activity, are capable of adsorbing numerous oxygen atoms on the surface[103]. The distributed oxygen atoms enable the capture of Ir single atoms through strong bonds. The introduction of single Ir atoms induces a synergistic effect with Co atoms in the substrate. Due to the disparate electron affinities of Ir and Co, high-concentration electrons migrate to the Ir site, promoting the adsorption of intermediates on the Ir site, thereby altering the adsorption Gibbs energy difference of different intermediates and achieving ultra-high activity oxygen evolution. Luo *et al.* also demonstrated the synergistic effect between Ir single atoms and Ni elements in amorphous substrates on OER[104]. The synthesized three-dimensional NiFeIr ternary amorphous catalyst exhibits unique morphology and ternary composition, providing many advantages in catalytic activity. In addition to the catalytic activity of Ir single atoms, the Ni-based shell structure is also the OER active center, and the synergistic effect between different catalytic centers promotes the improvement of OER performance. Insights from Li *et al.* shed light on the understanding of

multi-element synergistic catalysis[105]. They synthesized amorphous NiRu-LDH anchored Pt SAC, which benefits from the amorphous structure, featuring both NiRu-OH sites for hydrolysis dissociation and single Pt atom sites for hydrogen recombination. The synergy of multiple sites promotes efficient HER in alkaline media.

The characteristics of the amorphous substrate dictate the absence of long-range ordered structure, yet it exhibits short-range order. This short-range order extends only a few atomic distances and does not repeat periodically throughout the material. This flexible short-range ordered structure enables the regulation of catalytic activity by various structures. Lyu *et al.* fabricated 2D wrinkle-like iron-phosphomolybdic acid mineral hydrogel nanosheets with an amorphous layered structure[106]. Subsequently, they synthesized carbon-free single Fe-atom-dispersed heterostructured Mo-based nanosheets (Fe/SAs@Mo-based-HNSs) via phosphating. Fe/SAs@Mo-based-HNSs possess Fe single-atom sites and multiple heterostructures (MoP, MoP_2, MoO_2), prompting the authors to establish various models to calculate the reaction mechanism. The calculation results demonstrate that both single-phase and heterostructure interface models promote water decomposition (Volmer step). For the Heyrovsky step, except for MoP/MoP_2, the free energy of hydrogen adsorption in the heterostructure interface and the single-atom dispersion model is superior to that in the single-phase model. Even the <Mo top> and <Mo-P bridge> sites in the MoP_2/MoO_2 model have ΔG_{H^*} values close to 0 eV [Figure 6A]. The calculation and experimental results demonstrate the multi-component synergy effect of single-atom-loaded amorphous substrates on alkaline HER. The local special structure of amorphous materials can also influence mass transfer effects. Chen *et al.* synthesized a short-range ordered amorphous catalyst, facilitating the diffusion of oxygen to the active sites of atom-dispersed FeN_4 and FeN_5, thereby enhancing ORR activity[107]. Wang *et al.* synthesized a titanium oxide electrode loaded with Ir single atoms for the chlorine evolution reaction[108]. They discovered that amorphization of the titanium oxide on the electrode surface proved to be an effective strategy for adjusting the coordination environment of the Ir single atoms anchored on the Ti electrode. Following the amorphization process, the Ir single atom transitioned from a six-coordinated to a four-coordinated state. This change in the coordination environment resulted in varied binding strength with chloride ions, ultimately enhancing the activity of the chlorine evolution reaction. The study underscores the impact of the amorphous structure and slow water dissociation of titanium oxide on altering the mass transfer state on the electrode surface. The amorphous structure serves as a barrier, hindering the penetration of oxygen into the titanium substrate, thereby impeding titanium passivation and aiding in enhancing the stability of the catalytic process. This anti-passivation mechanism was elucidated through X-ray photoelectron spectroscopy (XPS)-assisted Ar ion etching, enabling a qualitative analysis of the ratio of O/Ti atoms on the electrode surface and subsurface. As depicted in Figure 6B and C, the surface oxygen ratio of Ir_1O_6 experienced a significant increase after the reaction, whereas that of Ir_1O_4 remained nearly unchanged.

Optimizing electronic structure

Amorphous substrates exhibit remarkable potential in adjusting the electronic structure of catalysts and enhancing electronic metal-support interactions (EMSIs). Defects and special structures on amorphous substrates can readily induce changes in the electronic structure of single atoms. Inspired by the ligand charge donation-acquisition balance strategy, Cheng *et al.* reported a Pt SAC anchored on amorphous TiB_xO_y[109]. Pt/TiB_xO_y, with its special Ti-B-O framework structure, facilitates strong bonding between Pt single atoms and B. This balanced electron transfer between B-O and B-Pt results in optimal hydrogen adsorption free energy [Figure 6D], leading to high HER activity. Xu *et al.* proposed that the robust interaction between the amorphous substrate and isolated Pt atoms allows for the adjustment of the electronic structure of Pt atoms, thereby stabilizing it[110]. To leverage this phenomenon, they employed hydrothermal and calcination methods to anchor various single atoms on amorphous MoO_x. Notably, the unsaturated platinum atom exhibits strong electron coupling with substrate defects, optimizing the
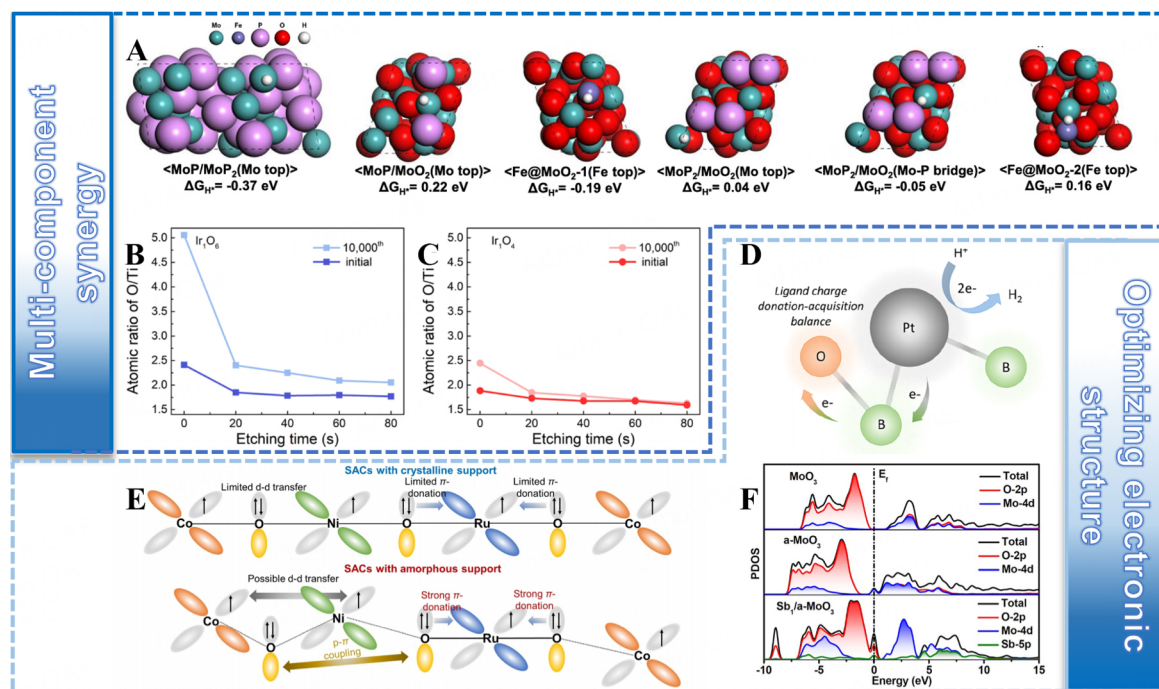
Figure 6. Amorphous substrates-assisted multi-component synergy and electronic structure optimization: (A) Representative atomic configurations after H*adsorption at the surface sites of MoP/MoP_2, MoP/MoO_2, MoP_2/MoO_2, Fe@MoO_2-1, and Fe@MoO_2-2, with corresponding ΔG_{H^*}. Reproduced with permission from Ref.[106] Copyright 2022, Springer Nature. (B) Atomic ratio of O/Ti on Ir_1O_6 after different etching times. (C) Atomic ratio of O/Ti on Ir_1O_4 after different etching times. Reproduced with permission from Ref.[108] Copyright 2024, American Chemical Society. (D) Electron transfer diagram of Pt/TiB_xO_y. Reproduced with permission from Ref.[109] Copyright 2022, American Chemical Society. (E) Schematic representations of the electronic coupling among Co-O-Ni-O-Ru-O-Co unit in amorphous and crystalline SACs. Reproduced with permission from Ref.[20] Copyright 2022, Wiley-VCH. (F) PODS of MoO_3, a-MoO_3, and Sb_y/a-MoO_3. Reproduced with permission from Ref[113]. Copyright 2023, American Chemical Society.

electronic structure of the Pt atom. This optimization leads to a reduction in the reaction barrier and enables ultra-high mass activity for the HER. Furthermore, this approach holds promise for the preparation of a range of amorphous SACs, offering exciting prospects for future applications. Hu *et al.* synthesized a FeCoNi-LDH anchored Ru SAC with an amorphous/crystalline hybrid structure[111]. This hybrid structure promotes electron transfer from Ru to Fe atoms and from Ni and Co to Ru atoms, optimizing the Ru site's electronic structure and enhancing OER activity. Understanding the influence of amorphous substrates on the electronic structure of the catalytic center is crucial for designing efficient electrocatalysts. By fine-tuning the electronic properties of the substrate and supporting single atoms, the adsorption intensity between the active center and key intermediates can be adjusted, thereby optimizing the reaction path for a specific reaction.

In amorphous substrates, structural disorder leads to a wide distribution of electron density of states, promoting orbital coupling and adjusting the position of the d-band center. This affects the adsorption energy of the intermediate, thereby influencing catalytic activity. Liu *et al.* prepared Ru single atoms uniformly dispersed on amorphous cobalt/nickel (oxy) hydroxide, resulting in different properties compared to Ru single atoms dispersed on crystal substrates[20]. High amorphization of the substrate induces orbital coupling and promotes electron transfer from Ru to nearby Co/Ni/O centers, enhancing water dissociation ability and regulating electron distribution of the local configuration [Figure 6E]. This reduces the oxygen affinity of the metal site and the affinity of the O site to H*, greatly promoting HER kinetics. Wang *et al.* introduced a large number of Fe atoms on amorphous $Zr(HPO_4)_2$, where the Fe atoms dispersed

on the surface of amorphous $Zr(HPO_4)_2$ have adjustable electron density[112]. Calculations show that the amorphous catalyst has a wider state density distribution and a lower d-band center, reducing the adsorption strength of oxygen-containing intermediates and improving OER performance. Chen *et al.* calculated the electronic structure of an amorphous MoO_3 catalyst loaded with Sb single atoms, revealing a wider density of state distribution in amorphous MoO_3[113]. This results in strong electronic interaction between Sb single atoms and amorphous MoO_3, leading to a smaller band gap and stronger occupied electronic state in $Sb_1/a-MoO_3$ [Figure 6F], accelerating electron transfer in nitric oxide electroreduction to ammonia process.

In summary, the interaction between the amorphous substrate and single atoms enhances the electrocatalytic reaction. These interactions distinguish amorphous SACs from crystalline SACs. Due to the higher defect density and disordered structural composition of the amorphous substrate, amorphous SACs possess various active sites, including single atoms and defects, and a range of heterostructures. This diversity aids in the adsorption and desorption of different reaction intermediates, providing more opportunities for optimizing the adsorption energy regulation of electrocatalytic reaction intermediates. Furthermore, because single atoms are more likely to interact with unique structures in amorphous substrates, amorphous SACs have advantages in adjusting the charge density of single atoms, modifying the energy band structure, and promoting orbital coupling compared to crystalline SACs [Figure 7]. Based on these characteristics and advantages, amorphous SACs are expected to see broader applications in the field of electrocatalysis in the future.

CONCLUSION AND OUTLOOK

Electrocatalysis offers a promising avenue for converting intermittent green energy sources such as solar and wind power into sustainable energy, laying the groundwork for robust energy storage and conversion systems. Amorphous materials, characterized by intrinsic defects and excellent catalytic performance, have garnered significant attention in electrocatalysis research. However, there remains a dearth of studies on SACs supported on amorphous substrates within this field. This review begins by summarizing the preparation techniques for amorphous substrates and elucidates the anchoring mechanisms and sites for single atoms. Subsequently, it highlights the interactions between single atoms and amorphous substrates based on existing literature. Compared to crystalline substrates, amorphous substrates offer distinct advantages, providing more anchoring sites for single atoms, preventing single-atom agglomeration, and fully exploiting the multi-component collaboration and electronic effects between the substrate and single atoms. Consequently, SACs supported on amorphous substrates often exhibit superior electrocatalytic performance. Despite the notable progress in this area, several challenges persist:

(1) Large-scale synthesis methods: Existing synthesis approaches for amorphous SACs are often inefficient in preparing amorphous substrates and anchoring single atoms. Simplified and universally applicable preparation methods are essential to meet the catalyst demands in practical applications.

(2) Accurate structural characterization methods: The complex local structure of amorphous materials necessitates more precise and comprehensive characterization techniques to delve deeper into the binding modes between single atoms and amorphous substrates and understand the precise local geometric structures of amorphous SACs. In addition, high facet SACs have abundant dislocations and defects, similar to amorphous SACs, which prevent single-atom aggregation and adjust the electronic structure. These properties need more comprehensive study. In the future, we can leverage the easier characterization of high facet SACs to thoroughly investigate the interaction mechanisms between high defect content substrates and single atoms. This research will further reveal the interaction mechanisms between amorphous substrates and single atoms.
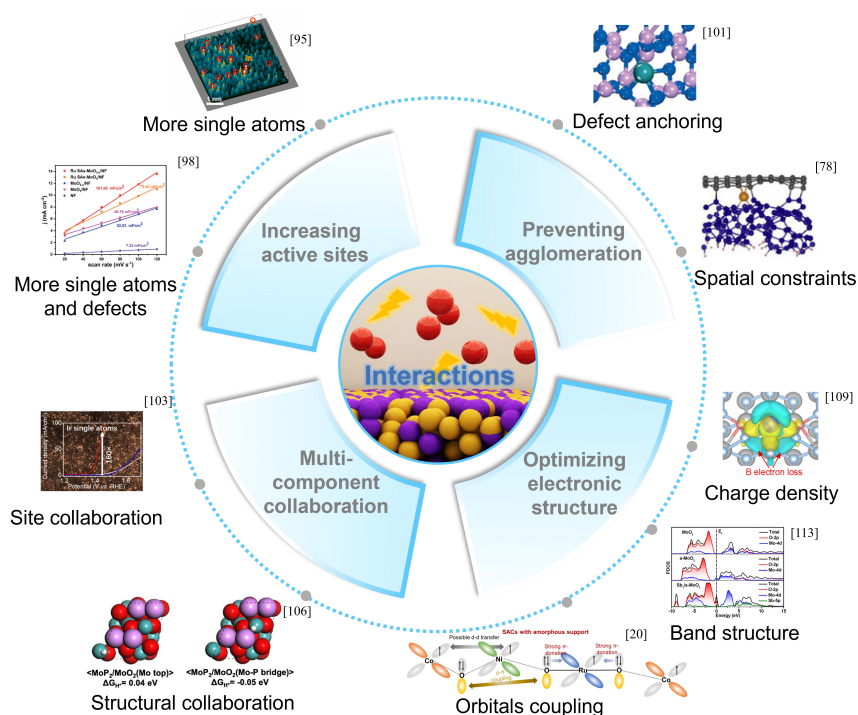
Figure 7. Summary of interactions between amorphous substrates and single atoms.

(3) *In-situ* structural transformation characterization: Amorphous SACs are susceptible to chemical structural transformations during reaction processes. *In-situ* techniques are required to monitor and elucidate the mechanisms of structural transformations.

(4) Improved calculation methods: The lack of long-range ordered structures in amorphous materials poses challenges in accurately modeling and calculating amorphous SACs. Hence, there is a pressing need for more accurate and rational calculation methods to analyze amorphous SACs and comprehend reaction mechanisms in detail.

Addressing these challenges will pave the way for further advancements in the development of amorphous SACs, leveraging their ultra-high atom utilization efficiency and the intrinsic activity of amorphous catalysts to create a range of catalyst families suitable for electrocatalysis and beyond.

DECLARATIONS
Authors' contributions
Conceived the review and wrote the manuscript: Zhou Y
Wrote the manuscript: Liu C, Cui Y

Availability of data and materials
Not applicable.

Conflicts of interest
All authors declared that there are no conflicts of interest.

Ethical approval and consent to participate
Not applicable.

Consent for publication
Not applicable.

Copyright

REFERENCES

1. Chu S, Majumdar A. Opportunities and challenges for a sustainable energy future. *Nature* 2012;488:294-303. DOI PubMed
2. Zhao D, Zhuang Z, Cao X, et al. Atomic site electrocatalysts for water splitting, oxygen reduction and selective oxidation. *Chem Soc Rev* 2020;49:2215-64. DOI
3. Zhang C, Luo Y, Tan J, et al. High-throughput production of cheap mineral-based two-dimensional electrocatalysts for high-current-density hydrogen evolution. *Nat Commun* 2020;11:3724. DOI PubMed PMC
4. Zhou Y, Zhou Q, Liu H, et al. Asymmetric dinitrogen-coordinated nickel single-atomic sites for efficient CO_2 electroreduction. *Nat Commun* 2023;14:3776. DOI PubMed PMC
5. Seh ZW, Kibsgaard J, Dickens CF, Chorkendorff I, Nørskov JK, Jaramillo TF. Combining theory and experiment in electrocatalysis: insights into materials design. *Science* 2017;355:eaad4998. DOI PubMed
6. Luo Y, Tang L, Khan U, et al. Morphology and surface chemistry engineering toward pH-universal catalysts for hydrogen evolution at high current density. *Nat Commun* 2019;10:269. DOI PubMed PMC
7. Wang A, Li J, Zhang T. Heterogeneous single-atom catalysis. *Nat Rev Chem* 2018;2:65-81. DOI
8. Yang H, Li G, Jiang G, Zhang Z, Hao Z. Heterogeneous selective oxidation over supported metal catalysts: from nanoparticles to single atoms. *Appl Catal B Environ* 2023;325:122384. DOI
9. Liu L, Corma A. Metal catalysts for heterogeneous catalysis: from single atoms to nanoclusters and nanoparticles. *Chem Rev* 2018;118:4981-5079. DOI PubMed PMC
10. Qiao B, Wang A, Yang X, et al. Single-atom catalysis of CO oxidation using Pt_1/FeO_x. *Nat Chem* 2011;3:634-41. DOI
11. Choi CH, Kim M, Kwon HC, et al. Tuning selectivity of electrochemical reactions by atomically dispersed platinum catalyst. *Nat Commun* 2016;7:10922. DOI PubMed PMC
12. Bruix A, Lykhach Y, Matolínová I, et al. Maximum noble-metal efficiency in catalytic materials: atomically dispersed surface platinum. *Angew Chem Int Ed* 2014;53:10525-30. DOI
13. Lin J, Wang A, Qiao B, et al. Remarkable performance of Ir_1/FeO_x single-atom catalyst in water gas shift reaction. *J Am Chem Soc* 2013;135:15314-7. DOI
14. Yang M, Allard LF, Flytzani-Stephanopoulos M. Atomically dispersed $Au-(OH)_x$ species bound on titania catalyze the low-temperature water-gas shift reaction. *J Am Chem Soc* 2013;135:3768-71. DOI PubMed
15. Zong L, Fan K, Wu W, et al. Anchoring single copper atoms to microporous carbon spheres as high-performance electrocatalyst for oxygen reduction reaction. *Adv Funct Mater* 2021;31:2104864. DOI
16. Choi J, Im S, Choi J, et al. Recent advances in 2D structured materials with defect-exploiting design strategies for electrocatalysis of nitrate to ammonia. *Energy Mater* 2024;4:400020. DOI
17. He J, Li N, Li Z, et al. Strategic defect engineering of metal-organic frameworks for optimizing the fabrication of single-atom catalysts. *Adv Funct Mater* 2021;31:2103597. DOI
18. Rong X, Wang HJ, Lu XL, Si R, Lu TB. Controlled synthesis of a vacancy-defect single-atom catalyst for boosting CO_2 electroreduction. *Angew Chem Int Ed* 2020;59:1961-5. DOI PubMed
19. Shi X, Huang Y, Bo Y, et al. Highly selective photocatalytic CO_2 methanation with water vapor on single-atom platinum-decorated defective carbon nitride. *Angew Chem Int Ed* 2022;61:e202203063. DOI
20. Liu Y, Liu X, Jadhav AR, et al. Unraveling the function of metal-amorphous support interactions in single-atom electrocatalytic hydrogen evolution. *Angew Chem Int Ed* 2022;134:e202114160. DOI
21. Zhou Y, Fan HJ. Progress and challenge of amorphous catalysts for electrochemical water splitting. *ACS Mater Lett* 2021;3:136-47. DOI
22. Chen D, Dong CL, Zou Y, et al. In situ evolution of highly dispersed amorphous CoO_x clusters for oxygen evolution reaction. *Nanoscale* 2017;9:11969-75. DOI

23.   Wang J, Han L, Huang B, Shao Q, Xin HL, Huang X. Amorphization activated ruthenium-tellurium nanorods for efficient water splitting. *Nat Commun* 2019;10:5692. DOI PubMed PMC

24.   Gebauer D, Cölfen H. Prenucleation clusters and non-classical nucleation. *Nano Today* 2011;6:564-84. DOI

25.   Chen G, Zhu Y, Chen HM, et al. An amorphous nickel-iron-based electrocatalyst with unusual local structures for ultrafast oxygen evolution reaction. *Adv Mater* 2019;31:e1900883. DOI

26.   Zhu Y, Liu C, Cui S, et al. Multistep dissolution of lamellar crystals generates superthin amorphous $Ni(OH)_2$ catalyst for UOR. *Adv Mater* 2023;35:e2301549. DOI

27.   Yang H, Chen Z, Guo P, Fei B, Wu R. B-doping-induced amorphization of LDH for large-current-density hydrogen evolution reaction. *Appl Catal B Environ* 2020;261:118240. DOI

28.   Kang Y, Henzie J, Gu H, et al. Mesoporous metal-metalloid amorphous alloys: the first synthesis of open 3D mesoporous Ni-B amorphous alloy spheres via a dual chemical reduction method. *Small* 2020;16:e1906707. DOI

29.   Cheng H, Yang N, Liu G, et al. Ligand-exchange-induced amorphization of Pd nanomaterials for highly efficient electrocatalytic hydrogen evolution reaction. *Adv Mater* 2020;32:e1902964. DOI

30.   Zhang X, Luo Z, Yu P, et al. Lithiation-induced amorphization of $Pd_3P_2S_8$ for highly efficient hydrogen evolution. *Nat Catal* 2018;1:460-8. DOI

31.   Wu G, Zheng X, Cui P, et al. A general synthesis approach for amorphous noble metal nanosheets. *Nat Commun* 2019;10:4855. DOI PubMed PMC

32.   Chen L, Jiang X, Wang N, Yue J, Qian Y, Yang J. Surface-amorphous and oxygen-deficient $Li_3VO_{4-\delta}$ as a promising anode material for lithium-ion batteries. *Adv Sci* 2015;2:1500090. DOI PubMed PMC

33.   Yang J, Li J, Wang T, et al. Novel hybrid of amorphous Sb/N-doped layered carbon for high-performance sodium-ion batteries. *Chem Eng J* 2021;407:127169. DOI

34.   Serrapede M, Savino U, Castellino M, et al. Li^+ Insertion in nanostructured TiO_2 for energy storage. *Materials* 2019;13:21. DOI PubMed PMC

35.   Zhang K, Su Q, Shi W, et al. Copious dislocations defect in amorphous/crystalline/amorphous sandwiched structure P-$NiMoO_4$ electrocatalyst toward enhanced hydrogen evolution reaction. *ACS Nano* 2024;18:3791-800. DOI

36.   Apostolova T, Obreshkov B. Femtosecond optical breakdown in silicon. *Appl Surf Sci* 2022;572:151354. DOI

37.   Jiang L, Tsai H. Repeatable nanostructures in dielectrics by femtosecond laser pulse trains. *Appl Phys Lett* 2005;87:151104. DOI

38.   Jiang L, Wang AD, Li B, Cui TH, Lu YF. Electrons dynamics control by shaping femtosecond laser pulses in micro/nanofabrication: modeling, method, measurement and application. *Light Sci Appl* 2018;7:17134. DOI PubMed PMC

39.   Zhao L, Chang B, Dong T, et al. Laser synthesis of amorphous CoS_x nanospheres for efficient hydrogen evolution and nitrogen reduction reactions. *J Mater Chem A* 2022;10:20071-9. DOI

40.   Liu Y, Liu C, Chen Z, et al. Fabrication of amorphous PdNiCuP nanoparticles as efficient bifunctional and highly durable electrocatalyst for methanol and formic acid oxidation. *J Mater Sci Technol* 2022;122:148-55. DOI

41.   McGee S, Lei Y, Goff J, et al. Single-step direct laser writing of multimetal oxygen evolution catalysts from liquid precursors. *ACS Nano* 2021;15:9796-807. DOI

42.   Zhang R, Zhao Y, Guo Z, Liu X, Zhu L, Jiang Y. Highly selective Pd nanosheet aerogel catalyst with hybrid strain induced by laser irradiation and P doping postprocess. *Small* 2023;19:e2205587. DOI

43.   Li B, Jiang L, Li X, et al. Controllable synthesis of nanosized amorphous MoS_x using temporally shaped femtosecond laser for highly efficient electrochemical hydrogen production. *Adv Funct Mater* 2019;29:1806229. DOI

44.   Budiyanto E, Zerebecki S, Weidenthaler C, et al. Impact of single-pulse, low-intensity laser post-processing on structure and activity of mesostructured cobalt oxide for the oxygen evolution reaction. *ACS Appl Mater Interfaces* 2021;13:51962-73. DOI PubMed PMC

45.   Lv C, Yan C, Chen G, et al. An amorphous noble-metal-free electrocatalyst that enables nitrogen fixation under ambient conditions. *Angew Chem Int Ed* 2018;57:6073-6. DOI

46.   Xi F, Bogdanoff P, Harbauer K, et al. Structural transformation identification of sputtered amorphous MoS_x as an efficient hydrogen-evolving catalyst during electrochemical activation. *ACS Catal* 2019;9:2368-80. DOI

47.   Qiao A, Tao H, Yue Y. Enhancing ionic conductivity in Ag_3PS_4 via mechanical amorphization. *J Non-Cryst Solids* 2019;521:119476. DOI

48.   Poryvaev AS, Polyukhov DM, Fedin MV. Mitigation of pressure-induced amorphization in metal-organic framework ZIF-8 upon EPR control. *ACS Appl Mater Interfaces* 2020;12:16655-61. DOI PubMed

49.   Sabochick MJ, Lam NQ. Radiation-induced amorphization of ordered intermetallic compounds CuTi, $CuTi_2$ and $CuTi_3$: a molecular-dynamics study. *Phys Rev B Condens Matter* 1991;43:5243-52. DOI

50.   Widmer RN, Lampronti GI, Casati N, Farsang S, Bennett TD, Redfern SAT. X-ray radiation-induced amorphization of metal-organic frameworks. *Phys Chem Chem Phys* 2019;21:12389-95. DOI PubMed

51.   Edinger M, Knopp MM, Kerdoncuff H, Rantanen J, Rades T, Löbmann K. Quantification of microwave-induced amorphization of celecoxib in PVP tablets using transmission Raman spectroscopy. *Eur J Pharm Sci* 2018;117:62-7. DOI PubMed

52.   Fei H, Dong J, Chen D, et al. Single atom electrocatalysts supported on graphene or graphene-like carbons. *Chem Soc Rev* 2019;48:5207-41. DOI PubMed

53.   Li M, Lv Q, Si W, Hou Z, Huang C. Sp-hybridized nitrogen as new anchoring sites of iron single atoms to boost the oxygen reduction

reaction. *Angew Chem Int Ed* 2022;61:e202208238. DOI PubMed

54.   Liu M, Wang X, Cao S, et al. Ferredoxin-inspired design of S-synergized Fe-Fe dual-metal center catalysts for enhanced electrocatalytic oxygen reduction reaction. *Adv Mater* 2024;36:e2309231. DOI

55.   Sun T, Zang W, Yan H, et al. Engineering the coordination environment of single cobalt atoms for efficient oxygen reduction and hydrogen evolution reactions. *ACS Catal* 2021;11:4498-509. DOI

56.   Zeng Z, Gan LY, Bin Yang H, et al. Orbital coupling of hetero-diatomic nickel-iron site for bifunctional electrocatalysis of CO_2 reduction and oxygen evolution. *Nat Commun* 2021;12:4088. DOI PubMed PMC

57.   Zhu Z, Yin H, Wang Y, et al. Coexisting single-atomic Fe and Ni sites on hierarchically ordered porous carbon as a highly efficient ORR electrocatalyst. *Adv Mater* 2020;32:e2004670. DOI

58.   Zhao X, Wang F, Kong XP, Fang R, Li Y. Dual-metal hetero-single-atoms with different coordination for efficient synergistic catalysis. *J Am Chem Soc* 2021;143:16068-77. DOI

59.   Ma X, Hu J, Zheng M, et al. N_2 reduction using single transition-metal atom supported on defective WS_2 monolayer as promising catalysts: a DFT study. *Appl Surf Sci* 2019;489:684-92. DOI

60.   Zhang Z, Feng C, Wang D, et al. Selectively anchoring single atoms on specific sites of supports for improved oxygen evolution. *Nat Commun* 2022;13:2473. DOI PubMed PMC

61.   He Q, Tian D, Jiang H, et al. Achieving efficient alkaline hydrogen evolution reaction over a Ni_5P_4 catalyst incorporating single-atomic Ru sites. *Adv Mater* 2020;32:e1906972. DOI

62.   Dong Q, Ma S, Zhu J, et al. Ultrahigh mass activity for the hydrogen evolution reaction by anchoring platinum single atoms on active {100} facets of TiC via cation defect engineering. *Adv Funct Mater* 2023;33:2210665. DOI

63.   Gong F, Liu Y, Zhao Y, et al. Universal sub-nanoreactor strategy for synthesis of yolk-shell MoS_2 supported single atom electrocatalysts toward robust hydrogen evolution reaction. *Angew Chem Int Ed* 2023;62:e202308091. DOI

64.   Elbakkay MH, El-Dek S, Farghali AA, El Rouby WM. Highly active atomic Cu catalyst anchored on superlattice CoFe layered double hydroxide for efficient oxygen evolution electrocatalysis. *Int J Hydrogen Energy* 2022;47:9876-94. DOI

65.   Zhang C, Cui Y, Yang Y, et al. Highly conductive amorphous pentlandite anchored with ultrafine platinum nanoparticles for efficient pH-universal hydrogen evolution reaction. *Adv Funct Mater* 2021;31:2105372. DOI

66.   Wang H, Bootharaju MS, Kim JH, et al. Synergistic interactions of neighboring platinum and iron atoms enhance reverse water-gas shift reaction performance. *J Am Chem Soc* 2023;145:2264-70. DOI

67.   Zhou Y, Song E, Chen W, et al. Dual-metal interbonding as the chemical facilitator for single-atom dispersions. *Adv Mater* 2020;32:e2003484. DOI

68.   Zhou Y, Hao W, Zhao X, et al. Electronegativity-induced charge balancing to boost stability and activity of amorphous electrocatalysts. *Adv Mater* 2022;34:e2100537. DOI

69.   Hannagan RT, Giannakakis G, Réocreux R, et al. First-principles design of a single-atom–alloy propane dehydrogenation catalyst. *Science* 2021;372:1444-7. DOI

70.   Zheng T, Liu C, Guo C, et al. Copper-catalysed exclusive CO_2 to pure formic acid conversion via single-atom alloying. *Nat Nanotechnol* 2021;16:1386-93. DOI

71.   Ji K, Xu M, Xu SM, et al. Electrocatalytic hydrogenation of 5-hydroxymethylfurfural promoted by a Ru_1 Cu single-atom alloy catalyst. *Angew Chem Int Ed* 2022;61:e202209849. DOI

72.   Li X, Shen P, Luo Y, et al. PdFe single-atom alloy metallene for N_2 electroreduction. *Angew Chem Int Ed* 2022;61:e202205923. DOI

73.   Han L, Ou P, Liu W, et al. Design of Ru-Ni diatomic sites for efficient alkaline hydrogen oxidation. *Sci Adv* 2022;8:eabm3779. DOI PubMed PMC

74.   Li P, Wang M, Duan X, et al. Boosting oxygen evolution of single-atomic ruthenium through electronic coupling with cobalt-iron layered double hydroxides. *Nat Commun* 2019;10:1711. DOI PubMed PMC

75.   Hou M, Zheng L, Zhao D, et al. Microenvironment reconstitution of highly active Ni single atoms on oxygen-incorporated Mo_2C for water splitting. *Nat Commun* 2024;15:1342. DOI PubMed PMC

76.   Wu Y, Ye C, Yu L, et al. Soft template-directed interlayer confinement synthesis of a Fe-Co dual single-atom catalyst for Zn-air batteries. *Energy Stor Mater* 2022;45:805-13. DOI

77.   Jiang Z, Zhou W, Hu C, et al. Interlayer-confined NiFe dual atoms within MoS_2 electrocatalyst for ultra-efficient acidic overall water splitting. *Adv Mater* 2023;35:e2300505. DOI

78.   Xi J, Sun H, Wang D, et al. Confined-interface-directed synthesis of palladium single-atom catalysts on graphene/amorphous carbon. *Appl Catal B Environ* 2018;225:291-7. DOI

79.   Loy ACM, Ng WL, Bhattacharya S. Advanced characterization techniques for the development of subatomic scale catalysts: one step closer to industrial scale fabrication. *Mater Today Catal* 2024;4:100033. DOI

80.   Ajayi TM, Shirato N, Rojas T, et al. Characterization of just one atom using synchrotron X-rays. *Nature* 2023;618:69-73. DOI

81.   Qi P, Wang J, Djitcheu X, He D, Liu H, Zhang Q. Techniques for the characterization of single atom catalysts. *RSC Adv* 2021;12:1216-27. DOI PubMed PMC

82.   Terban MW, Billinge SJL. Structural analysis of molecular materials using the pair distribution function. *Chem Rev* 2022;122:1208-72. DOI PubMed PMC

83.   Klingan K, Ringleb F, Zaharieva I, et al. Water oxidation by amorphous cobalt-based oxides: volume activity and proton transfer to electrolyte bases. *ChemSusChem* 2014;7:1301-10. DOI

84.   Tian H, Ma Y, Li Z, et al. Disorder-tuned conductivity in amorphous monolayer carbon. *Nature* 2023;615:56-61. DOI

85.   Su X, Wang Y, Zhou J, Gu S, Li J, Zhang S. Operando spectroscopic identification of active sites in NiFe prussian blue analogues as electrocatalysts: activation of oxygen atoms for oxygen evolution reaction. *J Am Chem Soc* 2018;140:11286-92. DOI

86.   Duan Y, Yu ZY, Hu SJ, et al. Scaled-up synthesis of amorphous NiFeMo oxides and their rapid surface reconstruction for superior oxygen evolution catalysis. *Angew Chem Int Ed* 2019;58:15772-7. DOI

87.   Zhang J, Yin R, Shao Q, Zhu T, Huang X. Oxygen vacancies in amorphous InO_x nanoribbons enhance CO_2 adsorption and activation for CO_2 electroreduction. *Angew Chem Int Ed* 2019;58:5609-13. DOI

88.   Yan J, Kong L, Ji Y, et al. Single atom tungsten doped ultrathin α-$Ni(OH)_2$ for enhanced electrocatalytic water oxidation. *Nat Commun* 2019;10:2149. DOI PubMed PMC

89.   Zhang R, Li Y, Zhou X, et al. Single-atomic platinum on fullerene C_{60} surfaces for accelerated alkaline hydrogen evolution. *Nat Commun* 2023;14:2460. DOI PubMed PMC

90.   Back S, Lim J, Kim NY, Kim YH, Jung Y. Single-atom catalysts for CO_2 electroreduction with significant activity and selectivity improvements. *Chem Sci* 2017;8:1090-6. DOI PubMed PMC

91.   Cheng N, Stambula S, Wang D, et al. Platinum single-atom and cluster catalysis of the hydrogen evolution reaction. *Nat Commun* 2016;7:13638. DOI PubMed PMC

92.   Zhang M, Xu W, Ma CL, Yu J, Liu YT, Ding B. Highly active and selective electroreduction of N_2 by the catalysis of Ga single atoms stabilized on amorphous TiO_2 nanofibers. *ACS Nano* 2022;16:4186-96. DOI

93.   Chen W, Ma Y, Li F, et al. Strong electronic interaction of amorphous Fe_2O_3 nanosheets with single-atom Pt toward enhanced carbon monoxide oxidation. *Adv Funct Mater* 2019;29:1904278. DOI

94.   Ma P, Feng C, Chen H, et al. Directing in-situ self-optimization of single-atom catalysts for improved oxygen evolution. *J Energy Chem* 2023;80:284-90. DOI

95.   Chen K, Zhang N, Wang F, Kang J, Chu K. Main-group indium single-atom catalysts for electrocatalytic NO reduction to NH_3. *J Mater Chem A* 2023;11:6814-9. DOI

96.   Liu W, Xu Q, Yan P, et al. Fabrication of a single-atom platinum catalyst for the hydrogen evolution reaction: a new protocol by utilization of H_xMoO_{3-x} with plasmon resonance. *ChemCatChem* 2018;10:946-50. DOI

97.   Shen R, Chen W, Peng Q, et al. High-concentration single atomic Pt sites on hollow CuS_x for selective O_2 reduction to H_2O_2 in acid solution. *Chem* 2019;5:2099-110. DOI

98.   Feng D, Wang P, Qin R, et al. Flower-like amorphous MoO_{3-x} stabilized Ru single atoms for efficient overall water/seawater splitting. *Adv Sci* 2023;10:e2300342. DOI PubMed PMC

99.   Liu C, Pan G, Liang N, Hong S, Ma J, Liu Y. Ir single atom catalyst loaded on amorphous carbon materials with high HER activity. *Adv Sci* 2022;9:e2105392. DOI PubMed PMC

100.   Zhang Q, Qin XX, Duan-Mu FP, et al. Isolated platinum atoms stabilized by amorphous tungstenic acid: metal-support interaction for synergistic oxygen activation. *Angew Chem Int Ed* 2018;57:9351-6. DOI

101.   Yang J, Chen B, Liu X, et al. Efficient and robust hydrogen evolution: phosphorus nitride imide nanotubes as supports for anchoring single ruthenium sites. *Angew Chem Int Ed* 2018;57:9495-500. DOI

102.   Hu Y, Chen C, Shen T, et al. Hollow carbon nanorod confined single atom Rh for direct formic acid electrooxidation. *Adv Sci* 2022;9:e2205299. DOI PubMed PMC

103.   Cai C, Wang M, Han S, et al. Ultrahigh oxygen evolution reaction activity achieved using Ir single atoms on amorphous CoO_x nanosheets. *ACS Catal* 2021;11:123-30. DOI

104.   Luo X, Wei X, Zhong H, et al. Single-atom Ir-anchored 3D amorphous NiFe nanowire@nanosheets for boosted oxygen evolution reaction. *ACS Appl Mater Interfaces* 2020;12:3539-46. DOI

105.   Li D, Chen X, Lv Y, et al. An effective hybrid electrocatalyst for the alkaline HER: highly dispersed Pt sites immobilized by a functionalized NiRu-hydroxide. *Appl Catal B Environ* 2020;269:118824. DOI

106.   Lyu F, Zeng S, Jia Z, et al. Two-dimensional mineral hydrogel-derived single atoms-anchored heterostructures for ultrastable hydrogen evolution. *Nat Commun* 2022;13:6249. DOI PubMed PMC

107.   Chen S, Zhang N, Narváez Villarrubia CW, et al. Single Fe atoms anchored by short-range ordered nanographene boost oxygen reduction reaction in acidic media. *Nano Energy* 2019;66:104164. DOI

108.   Wang J, Zhao L, Zou Y, et al. Engineering the coordination environment of Ir single atoms with surface titanium oxide amorphization for superior chlorine evolution reaction. *J Am Chem Soc* 2024;146:11152-63. DOI

109.   Cheng X, Xiao B, Chen Y, et al. Ligand charge donation-acquisition balance: a unique strategy to boost single Pt atom catalyst mass activity toward the hydrogen evolution reaction. *ACS Catal* 2022;12:5970-8. DOI

110.   Xu J, Zhang C, Liu H, et al. Amorphous MoO_X-stabilized single platinum atoms with ultrahigh mass activity for acidic hydrogen evolution. *Nano Energy* 2020;70:104529. DOI

111.   Hu Y, Luo G, Wang L, et al. Single Ru atoms stabilized by hybrid amorphous/crystalline FeCoNi layered double hydroxide for ultraefficient oxygen evolution. *Adv Energy Mater* 2021;11:2002816. DOI

112.   Wang R, Li Y, Tan X, et al. Amorphous doping promotes utilization of Fe-doped amorphous $Zr(HPO_4)_2$ for superb water oxidation electrocatalysis. *Adv Mater Inter* 2022;9:2200387. DOI

113.   Chen K, Zhang Y, Xiang J, Zhao X, Li X, Chu K. p-Block antimony single-atom catalysts for nitric oxide electroreduction to ammonia. *ACS Energy Lett* 2023;8:1281-8. DOI